JOURNAL OF MATERIALS SCIENCE **38** (2003) 1457– 1464

EPMA mapping of small particles of α-AlFeSi and β-AlFeSi in AA6063 alloy billets

YOSHIO OSADA
Nikkei Analytical Center Ltd., 1-34-1 Kambara, Ihara-gun, Shizuoka-ken 421-3203, Japan
E-mail: yoshio-osada@nikkeikin.co.jp

It is well known that the spatial distribution and the spatial density of the particles of α-AlFeSi and β-AlFeSi in the billets of Al-Mg-Si alloys, such as AA6063 alloys affect the quality of anodizing performance of their extrusions. For this reason it is very important to control the spatial distribution and the spatial density of both AlFeSi particles at extrusion plants. The X-ray diffraction method (XRD) has been used for discrimination between α-AlFeSi and β-ALFeSi particles. However it is not an appropriate method for determining the spatial distributions of particles in the alloys. As an alternative method an electron probe microanalyzer (EPMA) has been used for determining the spatial distributions of each element in the microstructures. However, unfortunately it is difficult to discriminate between the particles composed of the same elements like α-AlFeSi and β-AlFeSi particles. Thus, we tried to develop a convenient method to discriminate between α-AlFeSi and β-AlFeSi particles in the microstructure of AA6063 alloys and developed the EPMA mapping of α-AlFeSi and β-AlFeSi particles. First, in order to discriminate between the two particles, we tried to use the relative X-ray intensity ratio, the I_{Fe}/I_{Si} ratio instead of the Fe/Si mass ratio. Then, we calculated the value of the I_{Fe}/I_{Si} ratio from α-AlFeSi and β-AlFeSi by using Monte Carlo calculations and obtained the critical value of the I_{Fe}/I_{Si} ratio, to distinguish between α-AlFeSi and β-AlFeSi. After that, using the discrimination value, we developed the EPMA mapping program (EPMA method) to observe the distributions of α-AlFeSi and β-AlFeSi, and to calculate the areas (%) of α-AlFeSi and β-AlFeSi. Finally, we checked the correlation between the EPMA and the XRD methods. Consequently, the two methods were in good agreement. Today, this EPMA method instead of the XRD method is successfully used in the quality control of 6063 aluminum alloy billets after heat treatment at our aluminum extrusion works.

1. Introduction

It is well known that the spatial distribution and the density of the particles of α-AlFeSi ($Al_{8.3}Fe_2Si$) and β-AlFeSi ($Al_{8.9}Fe_2Si_2$) particles [1] the size of which are below 2 μm, in the billets of Al-Mg-Si alloys, such as AA6063 alloys affect the quality of anodizing performance of their extrusions. For this reason it is very important to control the spatial distribution and the density of both AlFeSi particles at extrusion plants. The X-ray diffraction method (XRD) has been used for the discrimination between α-AlFeSi and β-AlFeSi particles. However it is not an appropriate method for determining the distributions of particles in the alloys. As an alternative method an electron probe microanalyzer (EPMA) has been used for determining the distributions of each element in the microstructures. But unfortunately it is difficult to discriminate between the particles composed of same elements like α-AlFeSi and β-AlFeSi particles. Moreover, because quantitative analysis using EPMA is time consuming, it is impossible to continuously measure multiple targets. Also, if the target size is smaller than a generated X-ray region, the ZAF method cannot be used. Thus, we tried to develop a convenient method to discriminate between α-AlFeSi and β-AlFeSi particles in the microstructure of AA6063 alloys, based on a Monte Carlo calculation for EMPA. The Monte Carlo method for electron probe microanalysis has been investigated for many years. The studies of the thickness determination of thin films [3, 4], the coefficient of backscattered electrons [5, 6], the generation of secondary electrons [7–9], and the quantitative analysis of small particles [10], and so forth have been reported so far. However, the Monte Carlo methods have not been applied to the discrimination between the particles composed of the same element like α-AlFeSi and β-AlFeSi particles. Recently, personal computers have become to be used. In the case of using personal computers, the relationship between the calculation time and the acceptable error is one of the important factors. The recent study says the number of incident electrons can be reduced to about a few thousands in order to obtain the results within acceptable error [11]. In this study, moreover we tried to reduce the number of incident electrons. The present paper describes the development

process of the Monte Carlo calculation for EPMA and applications of the developed Monte Carlo calculation to the discrimination between α-AlFeSi and β-AlFeSi particles in the microstructures of AA6063 alloy billets with EPMA.

2. Mapping program of α-AlFeSi and β-AlFeSi particles

If we try to measure the spatial distributions of α-AlFeSi and β-AlFeSi particles in AA6063 alloy billets, we must develop the mapping program. For this purpose, here we develop the following three matters. The first is to develop a Monte Carlo calculation program to calculate the X-ray intensities from mixed targets. The second is to develop a method to discriminate between α-AlFeSi and β-AlFeSi particles. The third is to develop a mapping program.

2.1. Monte Carlo simulation model

2.1.1. Elastic scattering

A Monte Carlo simulation model for electron scattering in a solid is shown in Fig. 1. As seen in the figure, an incident electron collides with one of the elements constituting a mixed target and is elastically scattered by the angle of (ωn, ϕn). The intensity of generated X-rays from the mixed target is calculated along the step length (λn). For the intensity of the generated X-rays an absorption correction is carried out, and an electron energy loss through one step is calculated. These calculations are carried out for all steps of the electron and the amount of the X-ray intensities is integrated. The calculation is stopped either when the electron escaped from the mixed target into the vacuum space or when the electron energy was below the critical excitation energy. When an electron escaped from the target into vacuum space, the step length is divided. Also, the intensities of generated X-rays from particles are prorated corresponding to the step lengths divided. We used the screened Rutherford-type expression for elastic scattering of an incident electron. Then the scattering angle is determined, using a uniform random number R as shown by Equation 1 [12]

$$\cos\omega = 1 - 2\beta_i R/(1 + \beta_i - R) \tag{1}$$

where ω is the scattering angle (radian) of the electron and β_i is the screening parameter which is shown in the following section. A rotation angle ϕ is given by using another uniform random number R.

$$\phi = 2\pi R \tag{2}$$

The probability (P_i) of an electron scattered by an atom, i is given by Equation 3.

$$P_i = (\sigma_i \cdot C_i/A_i)/\Sigma(\sigma_i \cdot C_i/A_i) \tag{3}$$

The total cross section (σ^i_{tot}) of the atom is given by Equation 4.

$$\sigma^i_{tot} = \rho \cdot N_A \cdot \pi \cdot e^4 \Sigma[C_i/A_i \cdot Z_i(Z_i + 1)] /[\beta_i(\beta_i + 1)]/4E^2 \tag{4}$$

where A_i is the atomic weight, Z_i the atomic number, C_i the concentration in weight fraction, e the electron charge (-4.8029×10^{-10} esu), E (keV) electron energy, N_A Avogadro's number (6.02×10^{23}) and ρ (g/cm^3) the mass density. $\beta_i = [5.44Z_i^{2/3}/E \times 10^{-3}]$ [13]. When an elastic collision occurred in a mixed target, we must consider which atom scattered an incident electron. Here, a generated uniform random number R is shared as the proportional partition of the total cross section of each atom [12]. The expression is as follows for three elements of A,B and C. If $R \leqq P_A$, then the electron collides with an A atom. If $P_A < R \leqq P_A + P_B$, then the electron collides with a B atom. If $P_A + P_B < R \leqq P_A + P_B + P_C$, then the electron collides with a C atom.

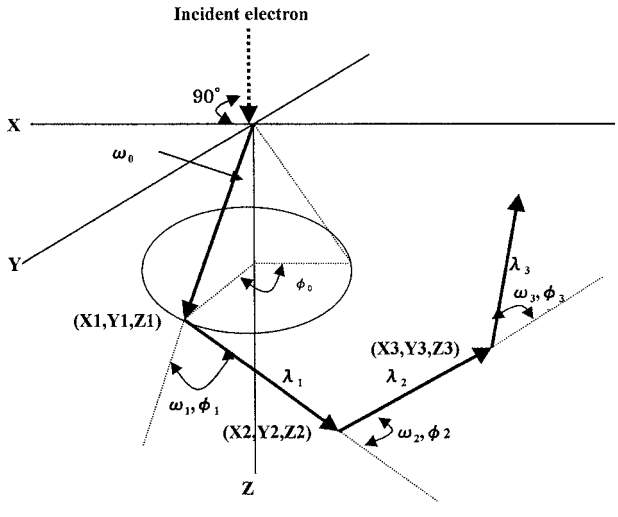

Figure 1 Monte Carlo simulation model for an electron scattering.

2.1.2. Energy loss

The stopping power of an electron in solids is given by Equation 5 [14] and Equation 6 [15].

$$\text{For} \quad E > 6.338\Sigma J_i C_i$$

$$\Delta E/\Delta S[\text{keV/cm}] = 7.85 \times 10^4 \rho \Sigma[Z_i C_i/A_i \cdot \ln(1.166E/J_i)]/E \tag{5}$$

$$\text{For} \quad E \leqq 6.338\,\Sigma J_i C_i$$

$$\Delta E/\Delta S[\text{keV/cm}] = 7.85 \times 10^4 \rho \Sigma\left(Z_i C_i/A_i/J_i^{1/2}\right)/1.26\text{E}^{1/2} \tag{6}$$

where $\Delta E/\Delta S$ is the stopping power of the electron (ΔS means a mean free path), and J_i is the mean ionization potential. J_i [Kev] $= 11.5Z_i \times 10^{-3}$ [16].

2.1.3. X-ray intensity

The characteristic X-ray intensity (I_i') generated at the nth step is given by Equation 7.

$$
\begin{aligned}
I_i' &= N_A Q_i(E) W_i C_i / Ai \cdot \lambda_n \\
Q_i(E) E_{ik}^2 &= 7.92 \times 10^{-20} \cdot \ln(U_i)/U_i \\
U_i &= E/E_{ik} \\
W_i &= \alpha^4/(1+\alpha^4) \\
\alpha &= -0.0217 + 0.032 Z_i - 1.14 Z_i^3 \times 10^{-6}
\end{aligned} \tag{7}
$$

where $Q_i(E)$ [17] is the ionization cross section for inner shell electrons, λ_n the mean free path, E_{ik} (keV) the excitation energy of the K shell electron of an i atom, and W_i [18] the fluorescence yield. After that, the X-ray intensities generated at nth step are carried out the absorption correction. Further, the relative X-ray intensity (IXp) is calculated by Equation 8.

$$
IX_p = \Sigma^m \Sigma^n IAn' / \Sigma^m \Sigma^n ISn' \tag{8}
$$

where IAn′ and ISn′ are the X-ray intensities from an A element in a target and a pure A element at the nth step, respectively. A superscript m is the number of incident electrons.

TABLE I Physical properties used in Monte Carlo calculation

Particle	Atom	Composition (mass %)	Density (g/cm^3)
α-AlFeSi	Al	62.0	3.5
	Fe	30.0	
	Si	8.0	
β-AlFeSi	Al	58.0	3.5
	Fe	27.0	
	Si	15.0	
Element	Al	100	2.7
	Fe	100	7.86
	Si	100	2.34

TABLE II Physical properties used in Monte Carlo calculation

Atom (Line)	Critical excitation voltage (keV)	Atomic number	Atomic weight	Absorption coefficient	
Al (Kα)	1.559	13	26.98	Al → Al	407
				Al → Fe	3420
				Al → Si	552
Fe (Kα)	7.11	26	55.847	Fe → Fe	76
				Fe → Al	99
				Fe → Si	124
Si (Kα)	1.838	14	28.08	Si → Al	3440
				Si → Fe	2490
				Si → Si	360

TABLE III Conditions of Monte Carlo calculation.

Number of incident electron	150
Accelerating voltage	15 kV
X-ray take-off angle	52.5°

2.2. Discrimination between α-AlFeSi and β-AlFeSi particles

To discriminate between α-AlFeSi and β-AlFeSi particles, we used the relative X-ray intensity of Fe/Si ratio, the I_{Fe}/I_{Si} ratio, instead of the Fe/Si mass ratio. We used the Monte Carlo method mentioned above to obtain the

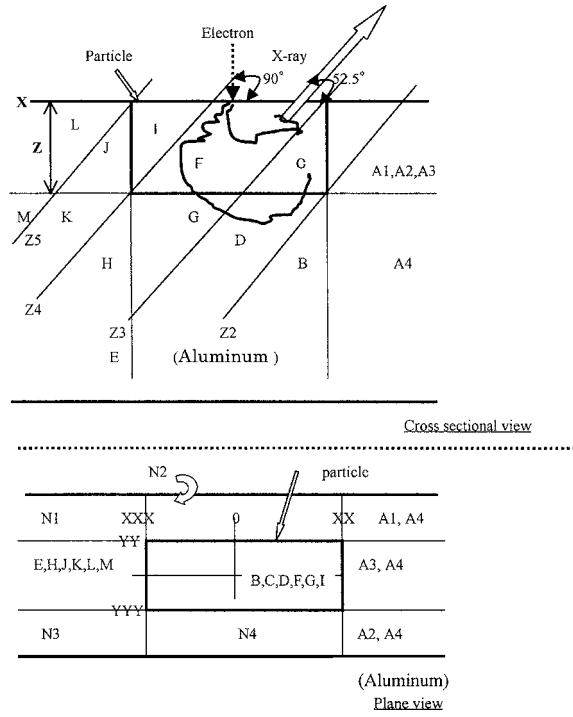

Figure 2 Modeling of X-ray absorption.

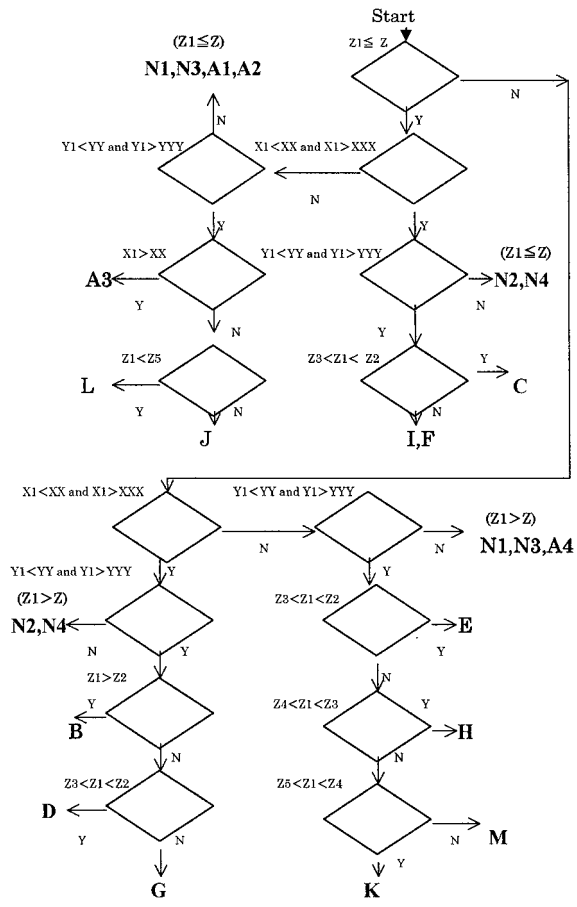

Figure 3 Procedure for the calculation of electron position.

TABLE IV Results of Monte Carlo calculation (α-AlFeSi)

	$X=0.2\ \mu$m, $Y=0.2\ \mu$m, $Z=0.2\ \mu$m				Bulk			
No.	I_{Fe}	I_{Si}	I_{Al}	I_{Fe}/I_{Si}	I_{Fe}	I_{Si}	I_{Al}	I_{Fe}/I_{Si}
1	0.0586	0.0087	0.9444	6.7	0.2835	0.0519	0.5254	5.5
2	0.0548	0.0085	0.9219	6.4	0.2729	0.0526	0.5270	5.2
3	0.0542	0.0077	0.9350	7.0	0.2753	0.0498	0.5208	5.5
4	0.0543	0.0079	0.9007	6.9	0.2770	0.0499	0.5099	5.5
5	0.0557	0.0083	0.9018	6.7	0.2796	0.0512	0.5063	5.5
6	0.0519	0.0079	0.9184	6.6	0.2704	0.0523	0.5305	5.2
7	0.0555	0.0082	0.9140	6.8	0.2782	0.0516	0.5104	5.4
8	0.0556	0.0084	0.9348	6.6	0.2705	0.0513	0.5151	5.3
9	0.0536	0.0078	0.9225	6.9	0.2843	0.0520	0.5298	5.5
10	0.0530	0.0081	0.9266	6.5	0.2797	0.0531	0.5361	5.3
Av	0.0547	0.0082	0.9220	6.7	0.2771	0.0516	0.5211	5.4
σ	0.0018	0.0003	0.0141	0.19	0.0049	0.0011	0.0011	0.13
CV (%)	3.2	3.7	1.5	2.8	1.8	2.1	2.0	2.4
Av -3σ	0.0493	**0.0073**	0.8797	5.4$\sim$	0.2624	0.0483	0.5178	**4.8**$\sim$
Av $+3\sigma$	0.0601	0.0091	0.9643	**8.2**	0.2918	0.0549	0.5244	6.0

CV (%) $= [\sigma/\text{Av}] \times 100$.

TABLE V Comparison between ZAF result and theoretical composition (α-AlFeSi)

	ZAF (mass %)			Relative error (%)		
No.	Fe	Si	Al	Fe	Si	Al
1	31.43	8.32	61.56	4.8	4.0	0.7
2	30.29	8.45	61.52	1.0	5.6	0.8
3	30.54	8.00	60.94	1.8	0	1.7
4	30.70	8.00	59.79	2.3	0	3.6
5	30.98	8.20	59.43	3.3	2.5	4.1
6	30.03	8.41	61.86	0.1	5.1	0.2
7	30.83	8.27	59.84	2.8	3.4	3.5
8	30.01	8.24	60.21	0	3.0	2.9
9	31.52	8.34	62.05	5.1	4.3	0.1
10	31.04	8.53	62.63	3.5	6.6	1.0
Av	30.73	8.28	60.98	2.5	3.5	1.9
σ	0.5293	0.1758	1.1047			
CV (%)	1.7	2.1	1.8			
Av-3σ	29.14	7.75	57.67	2.9$\sim$	3.1$\sim$	3.7$\sim$
Av$+3\sigma$	32.32	8.81	64.29	7.7	10.1	7.0

CV (%) $= [\sigma/\text{Av}] \times 100$.

I_{Fe}/I_{Si} ratio from α-AlFeSi and β-AlFeSi targets. For this purpose we developed the program to calculate the amounts of the X-ray intensities generated from mixed targets. Also, the program was written in the BASIC language. First, we calculated the X-ray intensities of the Fe Kα and the Si Kα lines from α-AlFeSi and β-AlFeSi targets and calculated the X-ray intensities of the Fe Kα and the Si Kα lines from pure iron and pure aluminum targets. Next, we calculated the relative X-ray intensities of Fe, I_{Fe}, and the relative X-ray intensities of S_i, I_{Si}, and moreover the I_{Fe}/I_{Si} ratios.

2.2.1. Conditions of Monte Carlo calculation

The geometrical shapes of α-AlFeSi and β-AlFeSi are commonly observed as a plate shape and a needle shape, respectively. Therefore, the particles were assumed to be a rectangular parallel piped and the lengths X, Y, Z of the rectangular parallel piped were varied from 0.2 to 10 μm (bulk), respectively. Also, the minimum size of 0.2 μm was selected because the particles below 0.2 μm do not affect the quality of anodizing performance of AA6063 alloys extrusions. When all lengths were 10 μm, the target was assumed to be a bulk. Also, the variation of Monte Carlo calculations was estimated by statistical errors of ten trials obtained by changing the initial value for random number generation. Physical properties used in the Monte Carlo calculation are shown in Tables I and II. The other conditions are shown in Table III. And also, for the intensities of the generated X-rays an absorption correction was carried out. The model of X-ray absorption is shown Fig. 2. A1, A2, A3, A4, N1, N2, N3, N4, B, C, D, E, F, G, H, I, J, K, L and M illustrated Fig. 2 show the electron position zone. Also, Z2, Z3, Z4 and Z5 show the straight line which have the inclination of the X-ray taking angle of 52.5degrees. The absorption correction is carried out corresponding to the electron zone, which is decided by the procedure shown in Fig. 3.

2.2.2. Results and discussion

Using the PC-9821 V12 of NEC, we calculated the values of the I_{Fe}, the I_{Si}, the I_{Al} and the I_{Fe}/I_{Si} ratio from α-AlFeSi and β-AlFeSi targets. To check the accuracy of the calculations, the average, the standard deviation (σ) and the coefficient of variation (CV%) of the results were calculated. And also, the accuracy of calculations was estimated by statistical errors of $\pm 3\sigma$. The results for the minimum and the bulk particle sizes are shown in Table IV and VI. As a result, the statistical variation values of the I_{Fe}/I_{Si} ratio were from 4.8 to 8.2 for α-AlFeSi targets and from 2.1 to 3.7 for β-AlFeSi targets and the coefficient of the variation (CV%) was below 3%. Also, the values of the relative X-ray intensity from the bulk target were transferred to mass% by ZAF correction. Here, we applied an absorption correction by Philibert, an atomic number correction by Poole and Thomas, and a fluorescence correction by Reed. Moreover we compared between the results of the ZAF correction and those of the theoretical

TABLE VI Results of Monte Carlo calculation (β-AlFeSi)

	$X=0.2\ \mu$m, $Y=0.2\ \mu$m, $Z=0.2\ \mu$m				Bulk			
No.	I_{Fe}	I_{Si}	I_{Al}	I_{Fe}/I_{Si}	I_{Fe}	I_{Si}	I_{Al}	I_{Fe}/I_{Si}
1	0.0510	0.0157	0.9458	3.2	0.2415	0.0911	0.4555	2.7
2	0.0479	0.0156	0.9256	3.1	0.2442	0.0995	0.4867	2.5
3	0.0481	0.0144	0.9571	3.3	0.2441	0.0944	0.4840	2.6
4	0.0482	0.0146	0.9271	3.3	0.2495	0.0971	0.4934	2.6
5	0.0486	0.0152	0.9529	3.2	0.2527	0.1007	0.4892	2.5
6	0.0465	0.0148	0.9478	3.1	0.2366	0.0970	0.4865	2.4
7	0.0484	0.0148	0.9170	3.3	0.2539	0.1025	0.4969	2.5
8	0.0483	0.0156	0.9311	3.1	02428	0.0969	0.4822	2.5
9	0.0493	0.0150	0.9350	3.3	0.2477	0.0955	0.4802	2.6
10	0.0475	0.0152	0.9353	3.1	0.2468	0.0980	0.4847	2.5
Av	0.0484	0.0151	0.9375	3.2	0.2460	0.0973	0.4839	2.5
σ	0.0012	0.0004	0.0130	0.09	0.0053	0.0032	0.0111	0.08
CV (%)	2.5	2.6	1.4	2.8	2.2	3.3	2.3	3.2
Av -3σ	**0.0448**	0.0139	0.8985	2.8∼	0.2301	0.0877	0.4506	**2.1**∼
Av $+3\sigma$	0.0520	0.0163	0.9765	**3.7**	0.2619	0.1089	0.5172	3.0

CV (%) = [σ/Av] × 100.

TABLE VII Comparison between ZAF result and theoretical composition (β-AlFeSi)

	ZAF (mass %)			Relative error (%)		
No.	Fe	Si	Al	Fe	Si	Al
1	26.86	14.20	52.78	0.5	5.3	9.0
2	27.21	15.52	56.11	0.8	3.5	3.3
3	27.19	14.76	55.87	0.7	1.6	3.7
4	27.79	15.17	56.95	2.9	1.1	1.8
5	28.14	15.68	56.53	4.2	4.5	2.5
6	26.39	15.17	55.97	2.3	1.1	3.5
7	28.27	15.97	57.36	4.7	6.5	1.1
8	27.05	15.13	55.62	0.2	0.9	4.1
9	27.58	14.90	55.52	2.1	0.7	4.3
10	27.49	15.29	55.96	1.8	1.9	3.5
Av	27.40	15.18	55.86	2.0	2.7	3.7
σ	0.5784	0.4966	1.230			
CV (%)	2.1	3.3	2.2			
Av -3σ	25.66	13.69	52.17	5.0∼	8.7∼	2.7∼
Av $+3\sigma$	29.14	16.67	59.55	7.9	11.1	10.0

CV (%) = [σ/Av] × 100.

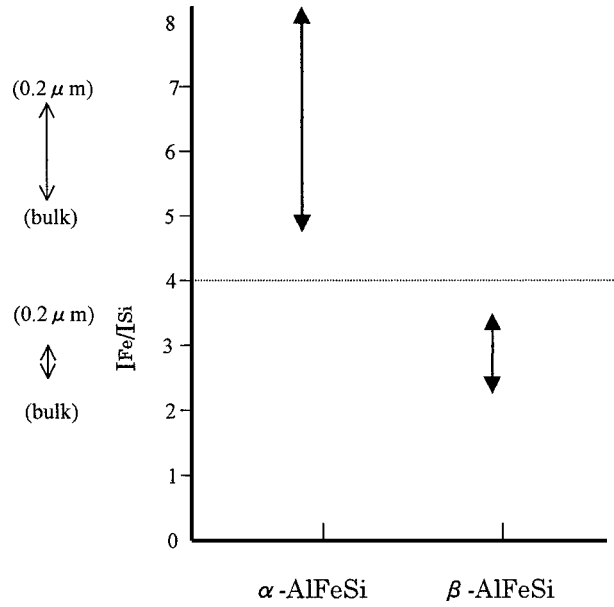

Figure 4 Results of calculation of I_{Fe}/I_{Si} ratio.

composition. The results are shown in Table V and VII. As a result, the coefficient of the variation (CV%) and the relative errors were below 3% and around 10%, respectively.

2.3. Discrimination value of I_{Fe}/I_{Si} ratio

The calculated results of the I_{Fe}/I_{Si} ratio are shown in Fig. 4. From the Fig. 4, the I_{Fe}/I_{Si} ratio was 4 or more for α-AlFeSi targets and less than 4 for β-AlFeSi targets. Consequently, the discrimination value of the I_{Fe}/I_{Si} ratio was 4.

3. Mapping program of α-AlFeSi and β-AlFeSi particles

Using the discrimination value of the I_{Fe}/I_{Si} ratio, we developed the mapping program of α-AlFeSi and β-AlFeSi particles for EPMA-8705 of Shimadzu Corporation. This mapping program can observe the spatial distributions and the spatial density of α-AlFeSi and β-AlFeSi particles in the microstructures of AA6063 alloys [19]. The program was written in the BASIC language.

4. Verification of mapping program

To verify the mapping program we developed, we compared the results of the EPMA method with those of the XRD method.

4.1. Samples for verification

We prepared four samples with different heat treatments as shown in Table VIII. The chemical composition of the aluminum billets is shown in Table IX and the samples were polished with a diamond paste. Also, we prepared a pure iron (99.99%) and a pure silicon (99.99%) as the standard samples provided by Shimadzu Corporation.

TABLE VIII Experimantal samples

Sample	Heat treatment
1	As cast
2	560°C × 2 hrs
3	580°C × 2 hrs
4	600°C × 2 hrs

TABLE IX Chemical composition of AA6063 alloys

mass%									
Fe	Si	Mg	Cu	Ti	Mn	Ni	Zn	Cr	Al
0.18	0.40	0.50	0.010	0.010	0.006	0.004	0.006	0.003	Bal.

TABLE X Measurement conditions of mapping

Accelerating voltage	15 kV
Sample current	20 nA for Al
Measuring time	0.5 sec/point
X-ray line (crystal)	Fe-Kα (LiF), Si-Kα (PET)
Take-off angle of X-ray	52.5°
Number of analysis point	200 × 200
Distance between adjacent analysis points	2 μm
Analysis area	400 μm × 400 μm
$I_{Fe} > 0.0448$ and $I_{Si} > 0.0073 \rightarrow \alpha$-AlFeSi or β-AlFeSi	
$I_{Fe}/I_{Si} \geqq 4 \rightarrow \alpha$-AlFeSi	
$I_{Fe}/I_{Si} < 4 \rightarrow \beta$-AlFeSi	

4.2. EPMA method

4.2.1. Mapping conditions

In order to carry out a night-time measuring, the measuring time (0.5 sec/point) and the number of analysis point (200 × 200) were used. Consequently, the measuring was about 8 hours. The distance between adjacent analysis points was set at 2 μm, because of the X-ray generation size f the plane direction for Al was around 2 μm. Namely, the analysis area is 400 μm × 400 μm. Moreover, when the I_{Si} and the I_{Fe} were larger than 0.0073 (Table IV, Av-3σ) and 0.0448 (Table VI, Av-3σ), we assumed the target is α-AlFeSi or β-AlFeSi particles. The summary of mapping conditions are shown in Table X.

4.2.2. Mapping results

We used the EPMA-8705 of Shimadzu Corporation and observed the X-ray images of α-AlFeSi and β-AlFeSi particles and measured their areas (%). Here, the areas (%) and the α ratio (%) are defined as follows.

Area (%) of α-AlFeSi
= [the number of analysis points detected as α-AlFeSi]/[the number of total analysis points] ×100

Area (%)of β-AlFeSi
= [the number of analysis points detected as β-AlFeSi]/[the number of total analysis points] ×100

α ratio (%)
= the area (%) from α-AlFeSi/[the area (%) from α-AlFeSi + the area (%) from β-AlFeSi] × 100

The results of the mapping are shown in Fig. 5. In the figure, the red contrast means α-AlFeSi particles and the blue contrast means β-AlFeSi particles. We can

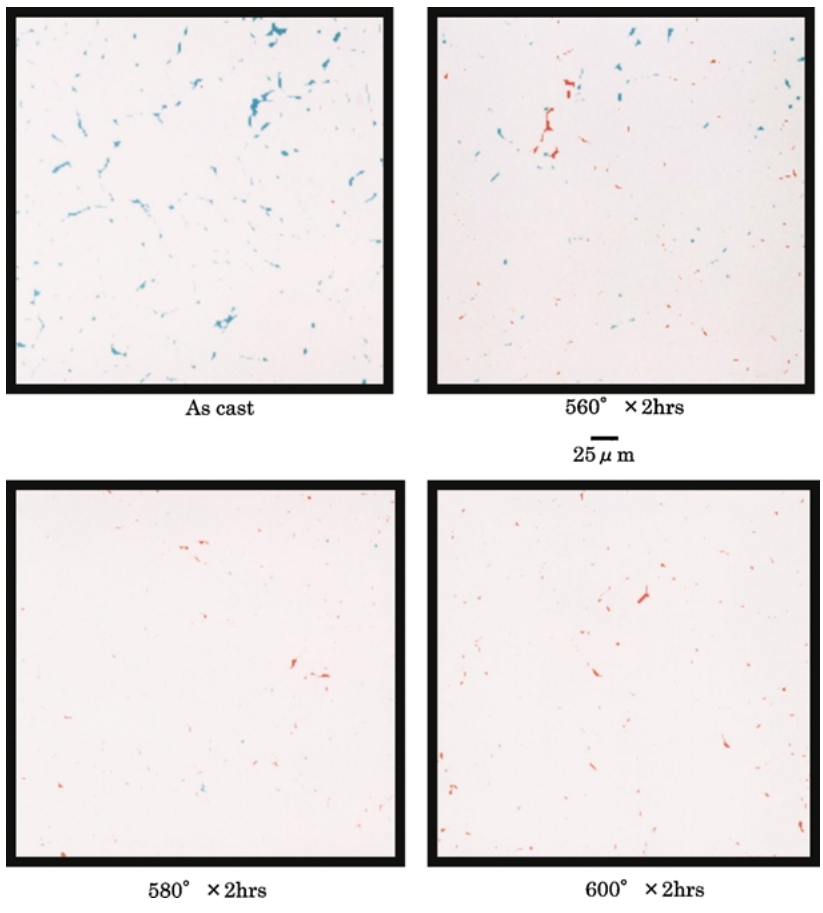

Figure 5 X-ray images of α-AlFeSi and β-AlFeSi.

TABLE XI Mapping results

	EPMA		
	Area (%)		
Heat treatment	α	β	α ratio (%)
As cast	4.36	0.07	2
560°C × 2 hrs	0.07	1.03	49
580°C × 2 hrs	1.16	0.25	82
600°C × 2 hrs	1.38	0.10	93

TABLE XII XRD results.

	XRD		
	X-ray intensity (kcps)		
Heat treatment	α	β	α ratio (%)
As cast	0.6	12.2	5
560°C × 2 hrs	2.8	4.2	40
580°C × 2 hrs	3.7	0.6	86
600°C × 2 hrs	4.6	0.1	98

observe the appearances of the distributed α-AlFeSi and β-AlFeSi particles, and also we can recognize that the amount of α-AlFeSi particles shown by the red contrast increases with an increase in temperature. On the other hand, the amount of β-AlFeSi particles shown by the blue contrast decreases with an increase in temperature. The values of the α ratio (%) are shown in Table XI.

4.3. XRD method

4.3.1. Measurement conditions

We used XRD (RAD-rB) of Rigaku Industrial Corporation. Cu Kα ($\lambda = 1.5418$ Å) X-rays were irradiated and the X-rays were generated at 50 kV and 200 mA.

4.3.2. Results

We measured the X-ray intensity of α-AlFeSi and β-AlFeSi and calculated the α ratio (%). Here, the α ratio (%) by XRD is defined as follows.

α ratio (%)
= the integrated X-ray intensity from α-AlFeSi / [the integrated X-ray intensity from α-AlFeSi + the integrated X-ray intensity from β-AlFeSi] × 100

The values of the α ratio (%) are shown in Table XII.

5. Discussion

The relationship between the EPMA and XRD methods is shown in Fig. 6. As described before, the definition of the α ratio (%) is strictly different between EPMA and XRD, namely, the EPMA method the area, on the other hand, the XRD method means the X-ray intensity. However, as shown in Fig. 6, the variations of the α ratio (%) obtained by EPMA and XRD were in good agreement.

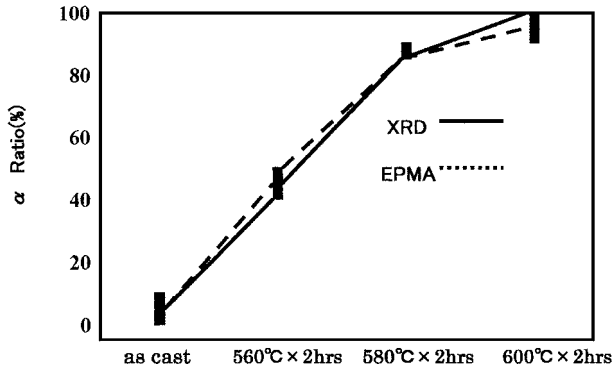

Figure 6 Comparison between EPMA and XRD.

6. Conclusions

1. Personal computers are effective in applications of the Monte Carlo method to EPMA analysis, where the number of incident electrons required is 150. The calculation time is below 2 minutes.

2. We can discriminate between α-AlFeSi and β-AlFeSi particles by the discrimination value (I_{Fe}/I_{Si} ratio) of 4. Namely, the I_{Fe}/I_{Si} ratio is 4 or more for α-AlFeSi particles and less than 4 for β-AlFeSi particles.

3. We can assume that this method is useful for the separation of small particles composed of the same elements, such as Al_2Cu and AlCu, Al_3Ti and AlTi, Al_3Mn and AlMn and so forth.

4. Although the results are satisfactory, there is a room to study about the discrimination of the particles lying below the surface.

5. Today, the EPMA method instead of the XRD method is successfully used in the quality control of AA6063 alloy billets after heat treatment at our aluminum extrusion works.

Acknowledgments

The author wishes to thank Professor Kenji Murata of Osaka Prefecture University for his valuable suggestions on Monte Carlo calculation and for his encouragement. Also, the author wishes to thank Mr. Shuichiro Watanabe for his metallurgic suggestions and Mr. Hideo Takada for the measurement of XRD. Finally, The author wishes to express that the reference samples were provided by Mr. Hiroshi Nagashima in Research and Development Center of Nippon Light Metal Co. Ltd.

References

1. G. RIVLIN and G. V. RAYNOR, *International Metals Reviews* **3** (1981) 133.
2. T. MINODA, H. HAYAKAWA and H. YOSHIDA, in Meeting of Japan institute of Light Metals, spring 1997.
3. K. MURATA, M. KOTERA and K. NAGAMI, *J. Appl. Phys.* **54**(2) (1983) 1110.
4. N. AMMANN and P. KARDUCK, *Surface and Interface Analysis* **22** (1994) 54.
5. P. G. T. HOWELL and A. BOYDE, *Scanning* **20** (1998) 45.
6. K. MURATA, *J. Appl. Phys.* **45**(9) (1974) 4110.
7. K. MURATA, D. F. KYSER and C. H. TING, *ibid.* **52**(7) (1981) 4396.
8. H. SEILER, *ibid.* **54** (1983) R1–R18.
9. DING ZE-JUN and R. SHIMIZU, *Scanning* **18** (1996) 92.

10. K. OOBORI, R. SHIMIZU, T. OURA and S. ICHIKAWA, *J. Appl. Phys.* **54**(1) (1983) 150.
11. K. OBORI *et al.*, *Jpn. J. Appl. Phys.* **41** (2002) 1616.
12. K. MURATA, T. MATSUKAWA and R. SHIMIZU, in Proceeding of the Sixth International Conference on X-ray Optics Microanalysis, Tokyo (1972) p. 105.
13. B. P. NIGAM, M. K. SAUNDERSON and WU. TA-YOU, *Phys. Rev.* **115** (1959) 491.
14. H. A. BETHE, *Ann. Physik* (*Leipzig*) **5** (1930) 325.
15. T. RAO-SAHIB and D. B. WITTRY, *J. Appl. Phys.* **45** (1974) 5060.
16. R. WILSON, *Phys. Rev.* **60** (1941) 749.
17. M. GREEN and V. E. COSSLETT, *Proc. Phys. Soc.* **78** (1961) 1206.
18. J. LABERRIGUE-FROLOW and P. RADVANYI, *J. Phys. Radium* **17** (1956) 944.
19. Y. OSADA, Patent application number 75487, 1999.

Received 17 April
and accepted 25 November 2002